Flame/Stretch Interactions of Premixed Hydrogen-Fueled Flames: Measurements and Predictions

O. C. KWON, and G. M. FAETH*

Department of Aerospace Engineering, The University of Michigan, Ann Arbor, MI 48109-2140, USA

Fundamental unstretched laminar burning velocities, and flame response to stretch (represented by the Markstein number) were considered both experimentally and computationally for laminar premixed flames. Mixtures of hydrogen and oxygen with nitrogen, argon and helium as diluents were considered to modify flame transport properties for computationally tractable reactant mixtures. Freely (outwardly)-propagating spherical laminar premixed flames were considered for fuel-equivalence ratios of 0.6 to 4.5, pressures of 0.3 to 3.0 atm, volumetric oxygen concentrations in the nonfuel gases of 0.21 to 0.36, and Karlovitz numbers of 0 to 0.5, at normal temperatures. For these conditions, both measured and predicted ratios of unstretched-to-stretched laminar burning velocities varied linearly with flame stretch (represented by the Karlovitz number), yielding constant Markstein numbers for particular reactant conditions. The present flames were very sensitive to flame stretch, exhibiting ratios of unstretched-to-stretched laminar burning velocities in the range 0.6 to 3.0 for levels of flame stretch well below quenching conditions. At fuel-lean conditions, increasing flame temperatures (by dilution with argon rather than nitrogen) tended to reduce flame sensitivity to stretch whereas increasing pressures tended to increase tendencies toward preferential-diffusion instability behavior. At low pressures, helium-diluted flames had reduced tendencies toward preferential-diffusion instability behavior compared to nitrogen- and argon-diluted flames due to stabilization of flame properties by strong effects of preferential diffusion of heat. Predicted and measured flame properties exhibited encouraging agreement using contemporary reaction mechanisms. Finally, flame structure predictions suggest that H and OH radical production and transport are important aspects of preferential-diffusion/stretch interactions, reflecting the strong correlation between laminar burning velocities and H+OH radical concentrations for present test conditions.

NOMENCLATURE

A = pre-exponential factor
D = mass diffusivity
E_a = activation energy
k = reaction coefficient
K = flame stretch or normalized increase of flame surface area, Eq. 3
Ka = Karlovitz number, KD_u/S_L^2
L = Markstein length
Ma = Markstein number, L/δ_D
Ma_{H+OH} = Markstein number based on $X_{(H+OH)max}$ in the reaction zone
n = power in reaction coefficient expression
p = pressure
r_f = flame radius
R = universal gas constant
S_L = laminar burning velocity based on unburned gas properties
$S'_{L\infty}$ = value of S_L at the largest radius observed
t = time
T = temperature
X_i = mole fraction of species i
δ_D = characteristic flame thickness, D_u/S_L
ϕ = fuel-equivalence ratio
ρ = density

Subscripts

b = burned gas
max = maximum observed value
u = unburned gas
∞ = unstretched flame condition

INTRODUCTION

It is widely recognized that flame/stretch interactions, due to preferential diffusion of various species and heat, can significantly affect the propagation velocities and structure of premixed flames [1–13], including strongly turbulent premixed flames typical of practical applications [14, 15]. Motivated by these observations, several studies of flame/stretch interactions of laminar

*Corresponding author. E-mail: gmfaeth@umich.edu

0010-2180/01/$–see front matter
PII 0010-2180(00)00229-7

COMBUSTION AND FLAME 124:590–610 (2001)

Published by Elsevier Science Inc.

premixed flames involving fuel oxidation by conventional air or oxygen-nitrogen mixtures were completed in this laboratory [16–22]. The objective of the present investigation was to modify the reactive and transport properties of computationally tractable reactant mixtures, involving some unconventional oxygen-diluent mixtures, so that both experiments and computations could be used to provide new perspectives to gain a better understanding of flame/stretch interactions. This was done by considering hydrogen and oxygen as reactants in the presence of several diluents: nitrogen to provide baseline results, argon to increase flame temperatures but with transport properties similar to nitrogen, and helium to increase both flame temperatures and transport rates (especially heat transfer rates compared to mass transfer rates) compared to nitrogen. Outwardly propagating spherical laminar premixed flames were used to measure fundamental laminar burning velocities of unstretched (plane) flames and the sensitivity of the laminar burning velocities to stretch (represented by Markstein numbers). Numerical simulations were carried out for the same flame configuration, based on detailed treatments of transport and chemical reaction properties and considering H_2/O_2 chemical reaction mechanisms due to Mueller et al. [23], Marinov et al. [24], and Frenklach et al. [25,26]. The predictions were evaluated using the new measurements.

Experimental and computational results were analyzed to find flame/stretch interactions similar to earlier studies in this laboratory [14–22]. This involved consideration of outwardly propagating spherical laminar flames at the thin-flame limit ($\delta_D/r_f < 2\%$) so that problems of flame thickness variations, curvature and unsteadiness caused by laminar burning velocity variations with the flame radius can be ignored [16, 17]. At such conditions, the relationship between laminar burning velocity and flame stretch can be conveniently represented by combining an early proposal of Markstein [2] and the "local conditions" hypothesis of Kwon et al. [15], to yield:

$$S_{L\infty}/S_L = 1 + MaKa \qquad (1)$$

The values of S_L and Ka were measured following Strehlow and Savage [3], based on predicted burned gas properties found using the computer codes of McBride et al. [27] and Reynolds [28]. The small stretch limit is also of interest, to connect present results at finite levels of stretch to classical asymptotic theories of laminar premixed flame propagation, as follows [17]:

$$S_L/S_{L\infty} = 1 - Ma_\infty Ka_\infty,\ Ka_\infty << 1 \qquad (2)$$

Fortuitously, both existing measurements and numerical simulations yield a linear correlation between $S_{L\infty}/S_L$ and Ka, for values of Ka not too near quenching conditions, which implies constant Markstein numbers for each reactant condition (mixture composition, pressure and temperature) [14–22]. In view of the complexity of laminar premixed flames a general proof of this constant Markstein number property is unlikely, however, once established for given conditions this behavior provides a very concise and helpful way of summarizing preferential-diffusion/stretch interactions. Other advantages of the "local conditions" hypothesis and Eq. 1 are discussed elsewhere [15–17].

Initial studies of flame/stretch interactions involving H_2 and O_2 as reactants are mainly limited to combustion in air and are reviewed by Aung et al. [17]. In addition, Aung et al. [17, 19] extended measurements for H_2 and O_2 flames to consider effects of pressure and nitrogen dilution on flame/stretch interactions and also completed numerical simulations of these flames finding reasonably good agreement between measurements and predictions based on the mechanisms of Frenklach et al. [25], Kim et al. [29], and Wang and Rogg [30]. Thus, the specific objectives of the present investigation were to consider further effects of pressure variations and dilution with nitrogen, argon and helium to modify the transport environment of the flames compared to past work. In addition, while continuing the evaluation of the chemical mechanism of Frenklach et al. [25], the more recent mechanisms of Mueller et al. [23], Marinov et al. [24], and Frenklach et al. [26] were considered during numerical simulations of flame properties.

The present discussion begins with descriptions of experimental and computational meth-

ods. Results are then considered, treating flame evolution and stability, burning velocity/stretch interactions, Markstein numbers, unstretched laminar burning velocities, flame structure, effects of pressure on flame properties, effects of flame temperature on flame properties, and effects of H and OH radical concentrations on flame behavior, in turn. The following discussion is brief, more details, and a complete tabulation of data, can be found in Kwon [31].

EXPERIMENTAL METHODS

Experimental methods are similar to past work and will be described only briefly, see [17–22] for more details. The experiments were conducted in a spherical windowed chamber having an inside diameter of 360 mm. The reactant mixture was prepared in the chamber by adding gases at appropriate partial pressures to reach the desired initial pressure. The gases were mixed using a small metal fan located within the chamber with motion allowed to decay before ignition (10 min for both mixing and decay). The combustible mixture was spark-ignited at the center of the chamber using minimum spark ignition energies to control ignition disturbances. The flames were observed using high speed (up to 7500 pictures per second) motion picture shadowgraphy. Once combustion was complete, the chamber was vented and then flushed with air to remove condensed water vapor and to cool the system to the allowable initial temperature range of the experiments (298 ± 3 K).

Present measurements were limited to flames having diameters larger than 10 mm to avoid ignition disturbances and smaller than 60 mm to limit pressure increases during the measuring period to values less than 0.7% of the initial pressure. No results were considered where the flame surface was distorted or wrinkled due to effects of buoyancy or flame instability. Similar to earlier work [15–22], measurements were limited to $\delta_D/r_f < 2\%$ so that effects of curvature and transient phenomena associated with large flame thicknesses were small. Finally, radiative heat losses were small (less than 0.2%) due to the large flame speeds of hydrogen-fueled flames and were ignored similar to past work. For these conditions, the laminar burning velocity and flame stretch are given as follows [3]:

$$S_L = (\rho_b/\rho_u)dr_f/dt,\ K = (2/r_f)dr_f/dt \qquad (3)$$

The density ratio needed to find S_L from Eq. 3 was computed assuming adiabatic constant-pressure combustion with the same concentrations of elements in the unburned and burned gases. These calculations were carried out using the adiabatic equilibrium algorithms of McBride et al. [27] and Reynolds [28], both yielding the same results. This is a *convention* that ignores preferential-diffusion effects that modify the local mixture fractions and thermal energy transport and cause local changes of the density ratios of stretched flames. The *convention* is convenient, however, because a single density ratio relates all flame speeds and laminar burning velocities, present methods are unchanged from earlier work that facilitates comparisons of measurements, and the approach retrieves the correct flame displacement velocity, dr_f/dt, for given unburned mixture conditions and Ka. Based on present numerical simulations (which will be shown to provide reasonably accurate predictions of flame properties), however, this effect is not very important for experimental results reported here. In particular, for acceptable experimental conditions ($\delta_D/r_f < 2\%$), predictions showed that ρ_b/ρ_u for stretched flames agreed with those for unstretched (plane) flames within 10% [31].

Final results were obtained by averaging mea-

TABLE 1

Summary of Hydrogen/Air Flame Test Conditions[a]

ϕ (−)	ρ_u/ρ_b (−)	$S_{L\infty}$ (mm/s)	Ka_{max} (−)	Ma (−)
0.60	5.56	820	0.11	−3.4
0.90	6.71	1,870	0.08	0.0
1.20	6.87	2,530	0.07	1.1
1.50	6.58	2,780	0.07	1.4
1.80	6.30	2,860	0.06	2.4
2.35	5.85	2,600	0.07	3.0
3.00	5.39	2,160	0.09	3.4
3.75	4.95	1,660	0.11	3.7
4.50	4.59	1,370	0.16	5.3

[a] Initial mixture pressure and temperature of 1 atm and 298 ± 3 K, $D_u = 72.9$ mm^2/s.

TABLE 2

Summary of $H_2/O_2/Ar$ Flame Test Conditions[a]

$O_2/(O_2 + Ar)$ (% vol.)	p (atm)	ϕ (−)	ρ_u/ρ_b (−)	$S_{L\infty}$ (mm/s)	Ka_{max} (−)	Ma (−)
21	0.3	0.60[b]	6.72	1,370	0.41	0.0
21	0.5	0.60	6.74	1,410	0.25	−0.1
21	0.5	4.50	4.97	1,690	0.50	4.2
21	1.0	0.60	6.78	1,450	0.11	−1.6
21	1.0	0.90	7.67	2,540	0.06	1.5
21	1.0	1.20	7.79	3,160	0.07	2.3
21	1.0	1.50	7.54	3,450	0.05	2.9
21	1.0	1.80	7.21	3,500	0.05	3.4
21	1.0	2.35	6.62	3,220	0.06	3.6
21	1.0	3.00	6.01	2,560	0.07	3.1
21	1.0	3.75	5.43	2,080	0.09	3.6
21	1.0	4.50	4.97	1,640	0.13	4.9
21	1.5	4.50	4.97	1,640	0.08	4.5
21	2.0	4.50	4.97	1,640	0.06	5.2
21	3.0	4.50	4.97	1,630	0.03	6.6
24	1.0	0.60	7.08	1,750	0.09	−1.6
24	1.0	4.50	5.08	1,810	0.13	4.8
27	1.0	0.60	7.30	2,190	0.09	−1.0
27	1.0	4.50	5.17	1,970	0.12	4.5
30	1.0	0.60	7.47	2,490	0.08	−0.9
30	1.0	4.50	5.24	2,210	0.10	5.3
33	1.0	0.60	7.60	2,970	0.06	0.0
36	1.0	0.60	7.69	3,470	0.05	0.5

[a] Initial mixture temperature od 298 ± 3 K, D_u = 76.9/p(atm) mm^2/s.

[b] Provisional results because $\delta_D r_f > 0.02$ for a portion of the database.

surements of 4 to 6 tests at each condition. Experimental uncertainties were estimated as described in [16] and references cited therein; the resulting experimental uncertainties (95% confidence) are as follows: S_L less than 9%, Ka less than 21%, $S_{L\infty}$ less than 10%, and |Ma| less than 25% for $|Ma| > 1$ and less than 25%/|Ma| for $|Ma| < 1$.

The experimental conditions and major results (D_u, ρ_u/ρ_b, $S_{L\infty}$, Ka_{max}, and Ma, where results to be discussed later show that Ma is constant for $Ka \leq Ka_{max}$) are summarized in Tables 1-3 for nitrogen-, argon- and helium-diluted hydrogen/oxygen flames, respectively. The total test range includes fuel-equivalence ratios of 0.6 to 4.5, pressures of 0.3 to 3.0 atm, volumetric oxygen concentrations in the nonfuel gases of 0.21 to 0.36 and Karlovitz numbers of 0 to 0.5, at normal temperatures. Some entries of Tables 1 through 3 are noted to be provided for information purposes only because they involve values of δ_D/r_f outside the allowable range.

TABLE 3

Summary of $H_2/O_2/He$ Flame Test Conditions[a]

ϕ (−)	ρ_u/ρ_b (−)	$S_{L\infty}$ (mm/s)	Ka_{max} (−)	Ma (−)
p = 0.5 atm:				
0.60[b]	6.74	2,280	0.34	0.6
p = 1.0 atm:				
0.60	6.78	2,620	0.12	1.1
0.90	7.67	3,710	0.12	1.5
1.20	7.79	4,200	0.11	1.9
1.80	7.21	4,350	0.12	2.3
2.35	6.62	3,940	0.13	2.3
3.00	6.01	3,170	0.16	2.7
3.75	5.43	2,540	0.23	3.2
4.50	4.97	1,980	0.38	3.7
p = 2.0 atm:				
0.60	6.80	2,720	0.07	0.4
4.50	4.97	1,870	0.13	3.2
p = 3.0 atm:				
0.60	6.82	2,640	0.04	−1.7
4.50	4.97	1,910	0.06	2.9

[a] Initial mixture temperature of 298 ± 3 K, $O_2/(O_2 + He)$ = 21% by volume, D_u = 158.7/p(atm) mm^2/s.

[b] Provisional results because $\delta_D/r_f > 0.02$ for a portion of the database.

COMPUTATIONAL METHODS

Numerical Simulations

Computational methods for the present flames were similar to Aung et al. [17, 19]. The outwardly propagating spherical laminar premixed flames were simulated using the unsteady one-dimensional laminar flame computer code RUN-1DL, developed by Rogg [32]. This algorithm allows for mixture-averaged multicomponent diffusion, thermal diffusion, variable thermochemical properties, and variable transport properties. The CHEMKIN package [33–35] was used as a preprocessor to find the thermochemical and transport properties for RUN-1DL. Transport properties were found from the transport property database of Kee et al. [35]; thermochemical properties were found from the thermodynamic database of Kee et al. [33], except for HO_2 where the recommendations of Kim et al. [29] were used. Before computing flame properties, all these properties were checked against original sources. Similar to the measurements, effects of radiation were small due to the large flame velocities of hydrogen-

TABLE 4

Corrections of Marinov et al. [24] Mechanism[a]

No.	Reaction	A	n	E_a
5b	$H + H + H_2 = H_2 + H_2$	9.20E + 16	−0.6	0.0
7	$H + O + M = OH + M$[b]	4.71E + 18	−1.0	0.0
8	$H + OH + M = H_2O + M$[b]	2.21E + 22	−2.0	0.0
10	$H + HO_2 = H_2 + O_2$	6.63E + 13	0.0	2.126
14	$OH + HO_2 = H_2O + O_2$[c]	2.13E + 28	−4.827	3.500
	$OH + HO_2 = H_2O + O_2$[c]	9.10E + 14	0.0	10.964

[a] H_2/O_2 reaction mechanism with equations numbered same as original source; all other equations unchanged from original source. Units are $cm^3/gmol/s/kcal/K$ and the reaction coefficient is taken as $k = AT^n \exp(-E_a/RT)$.

[b] Efficiency factors for the collison partners of this reaction are 6.4 for H_2O, all other species have efficiency factors of unity.

[c] This reaction is expressed as the sum of the two rate expressions.

fueled flames and were ignored. Flame propagation was allowed to proceed sufficiently far so that effects of initial conditions were small, similar to the measurements. Other limitations used to control experimental uncertainties, e.g., $\delta_D/r_f < 2\%$, etc., were also applied to the predictions. Finally, the computational grid in space and time was varied to ensure numerical accuracy within 1%, estimated by Richardson extrapolation of S_L. The numerical simulations were analyzed similar to the measurements, taking the flame position at the point where gas temperatures were the average of the hot and cold boundaries. Due to stringent flame thickness limitations, however, the results were not affected significantly by the criterion used to define the flame position.

Separate calculations were completed for unstretched (plane) flames using the steady one-dimensional laminar premixed flame code PREMIX, due to Kee and coworkers [36]. Other properties of these calculations, as well as levels of numerical accuracy, were the same as those using the RUN-1DL algorithm. This code was used to predict structure of unstretched flames and to obtain some properties of unstretched flames, e.g., the sensitivities of flames to effects of preferential diffusion of mass and heat.

Chemical Reaction Mechanism

Relatively recent H/O reaction mechanisms were considered during the present calculations, as follows: Mueller et al. [23], Marinov et al. [24], and Frenklach et al. [25, 26]. For the reaction mechanisms due to Frenklach et al. [25, 26], two versions were considered: GRI-Mech 2.1 and 3.0. C/H/O and N/O chemistry were not important for present conditions, similar to the findings of Aung et al. [17, 19], and were deleted from the mechanisms. Finally, an updated version of the mechanism of Marinov et al. [24] was used, see Table 4 for a summary of the specific changes from the original source.

The final reduced chemical reaction mechanisms, after incorporating the simplifications just discussed, involved 11 species and 19 reversible reactions for the approach of Mueller et al. [23], 20 reversible reactions for the approach of Marinov et al. [24], and 20 reversible reactions for the approach of GRI-Mech due to Frenklach et al. [25, 26] (not counting the range of third body collision efficiencies). The backward rates for all the mechanisms were found from chemical equilibrium requirements using the CHEMKIN package [34]. All the reaction mechanisms considered do not provide information about the elementary reactions including He and their reaction coefficients; hence the same reactions and their coefficients as those used for simulations of Ar-diluted hydrogen flames were chosen to compute He-diluted hydrogen flames due to the thermochemical similarities of Ar and He.

RESULTS AND DISCUSSION

Flame Stability and Evolution

Three kinds of flame surface instabilities were observed during the present investigation: pref-

erential-diffusion instability (when Ma < 0), hydrodynamic instability and buoyant instability. Shadowgraph photographs of flame surfaces after distortion by these instabilities for outwardly propagating spherical flames appear in Kwon et al. [15] and references cited therein. The presence of preferential-diffusion instability could be identified by irregular (chaotic) distortions of the flame surface relatively early in the flame propagation process. Preferential-diffusion instability was invariably observed when Markstein numbers were negative; fortunately, flame surfaces remained smooth at small radii even for unstable conditions so that laminar burning velocities could be measured for a time for these conditions. Hydrodynamic instability could be identified by the development of a somewhat regular cellular disturbance pattern on the flame surface, similar to observations of Groff [37]; fortunately, these instabilities generally were observed for flame diameters greater than 60 mm so that they did not affect present measurements. Finally, buoyant instability was readily detected by distortion of the flame surface from a spherical shape, as well as by upward motion of the centroid of the flame image. As noted earlier, no measurements were made when any of these instabilities were observed.

H_2/21% O_2/diluent (N_2, Ar, or He) Flames at NTP

Burning Velocity/Stretch Interactions

Results for finite flame radii involve finite values of flame stretch so that the laminar burning velocity at the largest r_f observed, $S'_{L\infty}$, still differs from the fundamental unstretched laminar burning velocity of a plane flame, $S_{L\infty}$. Thus, values of $S_{L\infty}$ were found from Eq. 1 by plotting $S'_{L\infty}/S_L$ as a function of Ka, similar to past work [15–22]. This yielded linear plots so that extrapolation to Ka = 0 gave $S'_{L\infty}/S_{L\infty}$ and thus $S_{L\infty}$, as summarized in Tables 1 through 3 for the measurements. Then given $S_{L\infty}$, plots of $S_{L\infty}/S_L$ as a function of Ka could be constructed for a given reactant mixture and pressure, as suggested by Eq. 1. Typical plots of this type are illustrated in Figs. 1 through 3 for hydrogen/air, H_2/21% O_2/Ar and H_2/21% O_2/He flames at normal temperature and pressure (NTP), respectively. Only some typical test conditions are illustrated in these figures; results at all the other test conditions are summarized in Tables 1 through 3 and are similar.

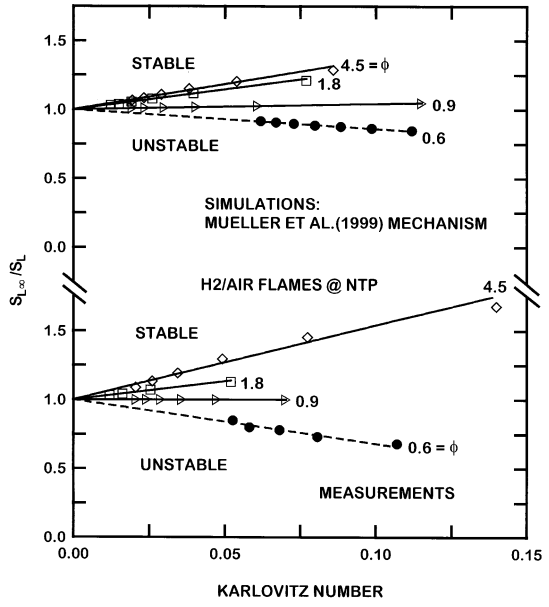

Fig. 1. Measured and predicted laminar burning velocities as a function of Karlovitz number and fuel-equivalence ratio for hydrogen/air flames at NTP. Predictions based on the kinetics of Mueller, et al. [23].

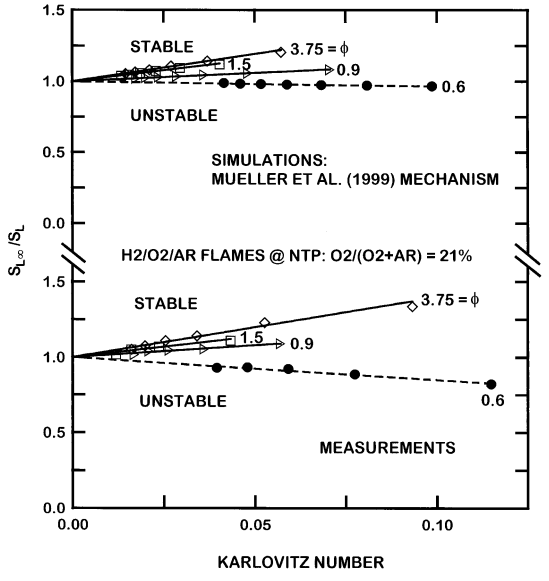

Fig. 2. Measured and predicted laminar burning velocities as a function of Karlovitz number and fuel-equivalence ratio for H_2/21% O_2/Ar flames at NTP. Predictions based on the kinetics of Mueller et al. [23].

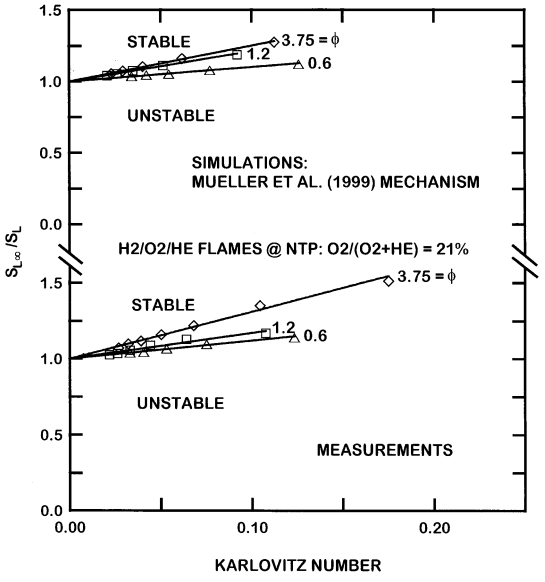

Fig. 3. Measured and predicted laminar burning velocities as a function of Karlovitz number and fuel-equivalence ratio for H_2/21% O_2/He flames at NTP. Predictions based on the kinetics of Mueller et al. [23].

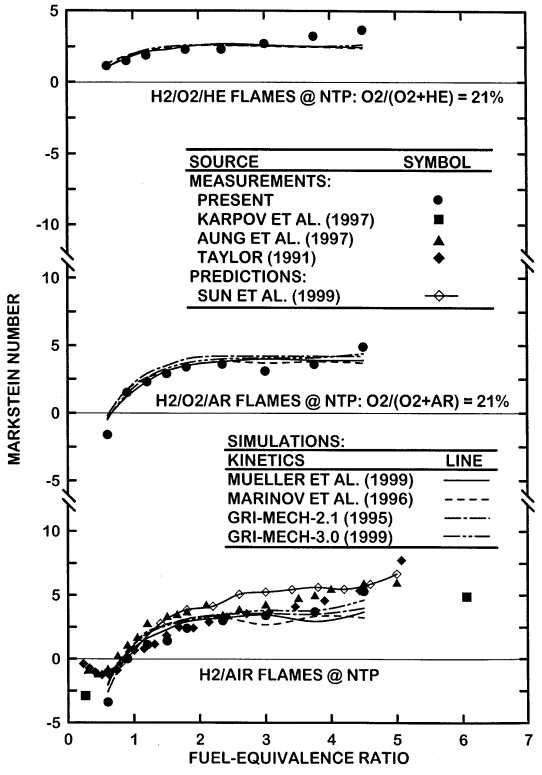

Fig. 4. Measured and predicted Markstein numbers as a function of fuel-equivalence ratio for hydrogen-fueled flames at NTP.

Results of both measurements and predictions illustrated in Figs. 1 through 3 exhibit the linear relationship between $S_{L\infty}/S_L$ and Ka that was exploited to find $S_{L\infty}$ well within experimental uncertainties; similar behavior was observed during earlier work [15–22]. Thus, the slope of each plot, which is equal to the Markstein number according to Eq. 1, is independent of Ka over the range of the measurements on these figures (which involves $Ka < 0.2$). Similar behavior was observed over the entire test range, which involves $Ka < 0.5$; however, quenching effects as extinction conditions are approached (where Ka would be on the order of unity, see Law [5]) would probably yield a more complex response to stretch. Even for the present modest range of Ka, however, effects of flame stretch on S_L were significant, e.g., over the entire test range, $S_{L\infty}/S_L$ varied in the range 0.6 to 3.0 for $Ka < 0.5$.

The predictions illustrated in Figs. 1 through 3 were based on the chemical reaction mechanism of Mueller et al. [23] but findings using the other chemical reaction mechanisms were qualitatively similar (and will be quantified when measured and predicted Ma are discussed in the next section). The results of the numerical simulations are seen to be qualitatively similar to the measurements, supporting both a linear variation of $S_{L\infty}/S_L$ with increasing Ka to yield constant Markstein numbers for each flame condition over the present test range and similar values of ϕ for unstable ($Ma < 0$) and stable ($Ma > 0$) preferential-diffusion behavior. However, the properties of preferential-diffusion/stretch interactions are seen most concisely from measured and predicted Markstein numbers, which are considered next.

Markstein Numbers

As discussed earlier, Markstein numbers are independent of Karlovitz numbers for present conditions and are summarized in Tables 1 through 3 as a function of reactant conditions. Measured and predicted values of Markstein numbers for H_2/21% O_2/diluent (N_2, Ar or He) flames at NTP are plotted as a function of fuel-equivalence ratio in Fig. 4.

Measurements of Markstein numbers for hy-

drogen/air flames at NTP illustrated in Fig. 4 include the results of Taylor [6], Karpov et al. [9], Aung et al. [17], and the present investigation. Predictions shown on the plot include results of Sun et al. [13], using a simplified integral method, and the present investigation. Over the range of conditions where $\delta_D/r_f < 2\%$, the various measurements agree within experimental uncertainties. Outside this range for very lean $\phi < 0.60$ and very rich $\phi > 5.0$ flames, discrepancies among the various measurements become relatively large, reflecting the larger experimental uncertainties and the intrusion of other effects, e.g., transient phenomena, buoyancy, radiative heat losses, etc., on measured values of Markstein numbers. All the measurements and predictions are in reasonably good agreement for fuel-lean conditions. Discrepancies among the predictions are somewhat larger at fuel-rich conditions with present predictions using all three mechanisms being somewhat smaller than the predictions of Sun et al. [13]. Earlier predictions of Aung et al. [17], using the same Kim et al. [29] mechanism as Sun et al. [17], are also similar to the present results; therefore, the reason for these differences is unknown. The general characteristics of unstable behavior ($Ma < 0$) at fuel-lean conditions and stable behavior ($Ma > 0$) at fuel-rich conditions are consistent with conventional explanations of flame stability based on preferential diffusion of the deficient reactant, see Kwon et al. [15] and Aung et al. [17] and references cited therein. Behavior at intermediate conditions (between $\phi \approx 0.9$ where $Ma = 0$ and $\phi \approx 1.8$ where $S_{L\infty}$ reaches a maximum) is more complex and, as will be shown later, involves preferential diffusion of both heat and mass. Another interesting feature of the results illustrated in Fig. 4 is the extended region where Ma varies slowly between $\phi \approx 2$ and 5 even although present experiments did not approach flammability limits. It is encouraging that the numerical simulations based on detailed chemical mechanisms can reproduce these trends, even although Markstein numbers were not used during past efforts to optimize the chemical kinetic parameters used in these mechanisms.

Corresponding measurements and predictions of Markstein numbers for hydrogen-fueled flames when nitrogen is replaced by argon or helium at NTP are also illustrated in Fig. 4. Only measurements and predictions from the present study are available for these conditions. Comparing the plots for the argon- and nitrogen-diluted flames shows that replacing nitrogen with argon has remarkably little effect on either the trends or magnitudes of the Markstein numbers even although the argon-diluted flames have significantly increased flame temperatures due to the smaller specific heats of argon compared to the nitrogen. This small effect on Ma of replacing nitrogen with argon is mainly due to the similar transport properties of the two flames, e.g., $D_u = 72.9$ mm^2/s for nitrogen-diluted flames at NTP whereas $D_u = 76.9$ mm^2/s for argon-diluted flames at NTP. Computations using all four mechanisms reproduce this behavior very well, which is encouraging.

In contrast to the previous observations of flame properties if nitrogen is replaced by argon, comparing the plots for helium- and nitrogen-diluted flames in Fig. 4 shows that replacing either nitrogen or argon by helium has a significant effect on Markstein numbers at fuel-lean conditions. In particular, using helium as the diluent stabilizes the fuel-lean flames mainly due to enhanced diffusion of heat. This occurs because the transport properties of helium-diluted flames are significantly different from those of nitrogen-diluted and argon-diluted flames, e.g., the mass diffusivity is increased ($D_u = 158.7$ mm^2/s for helium-diluted flames at NTP) but a more significant effect is the increase of thermal diffusivity of the mixture in the helium-diluted environment through the enhanced thermal conductivity of helium (roughly five times larger than that of nitrogen in the temperature range 300-3000 K). Thus, only stable preferential-diffusion behavior was observed for helium-diluted hydrogen flames at NTP over the all fuel-equivalence ratios considered during the present work; notably, present predictions represent this effect quite well.

Unstretched Laminar Burning Velocities

In the following, measured values of laminar burning velocities will be limited to recent results that have been corrected to provide $S_{L\infty}$.

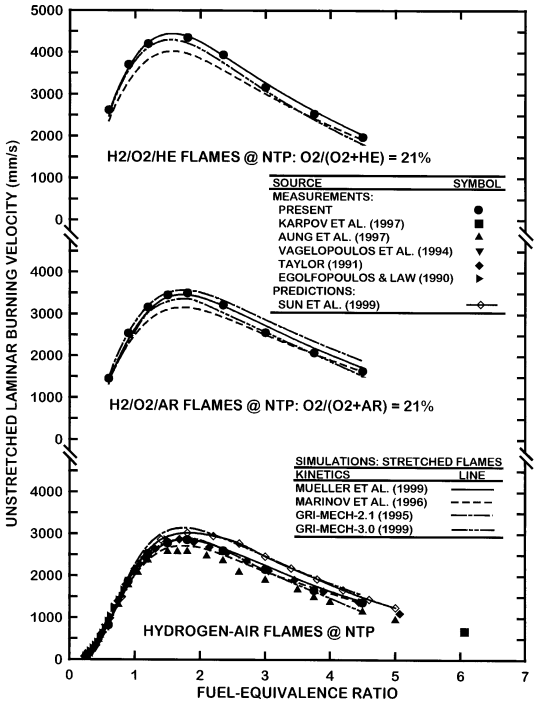

Fig. 5. Measured and predicted unstretched laminar burning velocities as a function of fuel-equivalence ratio for hydrogen-fueled flames at NTP.

The measured values of $S_{L\infty}$ are summarized in Tables 1 through 3, and measurements and predictions of $S_{L\infty}$ as a function of fuel-equivalence ratio for H_2/21% O_2/diluent (N_2, Ar or He) flames at NTP are plotted in Fig. 5.

Measurements of $S_{L\infty}$ for hydrogen/air flames at NTP illustrated in Fig. 5 include the results of Taylor [6], Karpov et al. [9], Egolfopoulos and Law [11], Vagelopoulos et al. [12], Aung et al. [17], and the present investigation. The results of Taylor [6] were found using freely (outwardly)-propagating spherical laminar premixed flames but with a different extrapolation procedure than the present investigation to estimate results for plane flame conditions. Karpov et al. [9] also measured unstretched laminar burning velocities and Markstein numbers for hydrogen/air flames at NTP, based on data reduction methods similar to the present methods, but their measurements were limited to only very fuel-lean and fuel-rich conditions. The measurements of Egolfopoulos and Law [11] and Vagelopoulos et al. [12] involved a different extrapolation procedure to estimate the laminar burning velocities of unstretched (plane) flames based on measurements using the counterflow twin-flame technique. Predictions shown on the plot include the results of Sun et al. [13] for unstretched flames using an integral method and the mechanism of Kim et al. [29] as well as present predictions based on the reaction mechanisms of Mueller et al. [23], Marinov et al. [24] and Frenklach et al. (GRI-Mech 2.1 [25], GRI-Mech 3.0 [26]) found by extrapolating results for simulations of outwardly propagating spherical flames similar to the measurements. It should be noted that the mechanism of Kim et al. [29] was used by Aung et al. [17] and is an earlier version of Mueller et al. [23] used during the present investigation. The measurements generally agree within experimental uncertainties. In addition, the measurements and all the predictions are in good agreement for fuel-lean conditions. At fuel-rich conditions, however, predictions using the mechanisms of GRI-Mech 2.1 (Frenklach et al. [25]) and Sun et al. [13] are somewhat larger than the measurements. On the other hand, predictions using the mechanism of GRI-Mech 3.0 (Frenklach et al. [26]) are surprisingly good even although this mechanism was not particularly tailored for hydrogen-fueled flames. Finally, the predictions of Sun et al. [13] are very similar to the earlier predictions of Aung et al. [17] using the same mechanism in conjunction with a numerical simulation of the propagating flame.

Measurements of laminar burning velocities were carried out after replacing the nitrogen in air with argon. As mentioned earlier, the specific heats of argon are smaller than nitrogen, which provides a way to consider effects of larger flame temperatures on flame/stretch interactions, however, in the previous section it was shown that the resulting effect of the larger flame temperature on Ma is small. The corresponding measurements and predictions of $S_{L\infty}$ as a function of fuel-equivalence ratio for the argon-diluted flames are plotted in Fig. 5. Only results from the present study are available for argon dilution, with the four predictions obtained from the mechanisms of Mueller et al. [23], Marinov et al. [24] and Frenklach et al. (GRI-Mech 2.1 [25], GRI-Mech 3.0 [26]). Comparing the plots for the nitrogen-diluted and argon-diluted flames shows that replacing nitro-

gen with argon causes roughly a 25% increase of the maximum unstretched laminar burning velocity but little change in the value of the fuel-equivalence ratio where the maximum is observed, e.g., $\phi \approx 1.8$. All the predictions reproduce this trend but the mechanism of Mueller et al. [23] provides the best quantitative predictions over the entire test range.

Measurements of laminar burning velocities were also carried out by replacing the nitrogen in air with helium. Similar to argon, the specific heats of helium are smaller than nitrogen, which increases flame temperatures; in addition, transport rates are larger in helium-diluted flames than in argon-diluted flames. The corresponding measurements and predictions of $S_{L\infty}$ as a function of fuel-equivalence ratio are also plotted in Fig. 5. Similar to the argon-diluted flames, only results from the present study are available for helium dilution, with the three predictions obtained using the mechanisms of Mueller et al. [23], Marinov et al. [24] and GRI-Mech 3.0 (Frenklach et al. [26]). Comparing the plots for the nitrogen- and helium-diluted flames shows that replacing nitrogen with helium causes roughly a 55% increase of the maximum unstretched laminar burning velocity but little change in the value of the fuel-equivalence ratio where the maximum is observed, e.g., $\phi \approx 1.6$ compared to $\phi \approx 1.8$ for hydrogen/air flames. This significant increase of $S_{L\infty}$ is due to both increased flame temperatures and transport rates. All the predictions reproduce this trend but the mechanism of Mueller et al. [23] is still seen to provide the best quantitative predictions over the entire test range of Fig. 5.

Finally, it is interesting to study the effect of stretch on the variation of laminar burning velocities as a function of fuel-equivalence ratio. In particular, the variation of S_L with fuel-equivalence ratio at a constant finite level of stretch is an example of one type of stretch environment that might have affected earlier observations of stretch-uncorrected laminar burning velocities (that involved unknown levels of stretch). Thus, measured and predicted laminar burning velocities at three levels of stretch (Ka = 0, 0.08 and 0.16), which are far from extinction conditions, are illustrated in Fig. 6 for H_2/21% O_2/Ar and H_2/21% O_2/He flames at

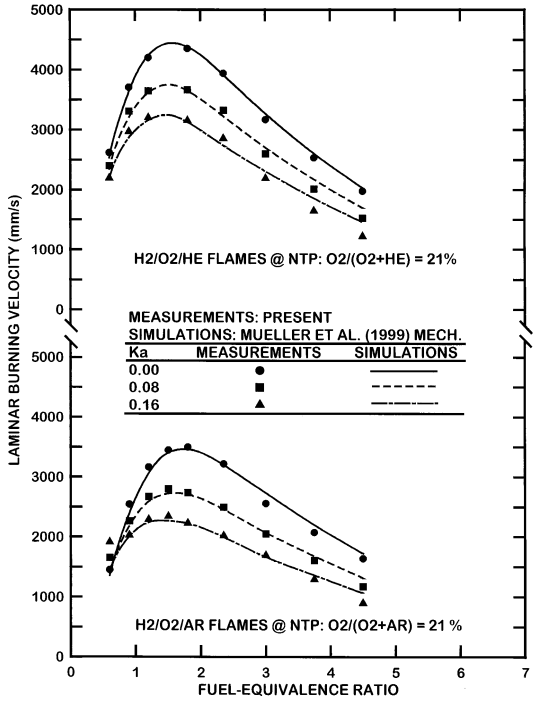

Fig. 6. Measured and predicted laminar burning velocities as a function of fuel-equivalence ratio at various stretch levels for H_2/21% O_2/diluent (Ar or He) flames at NTP. Predictions based on the kinetics of Mueller et al. [23].

NTP. As expected, this plot shows that laminar burning velocities decrease (increase) with increasing stretch levels for stable (unstable) preferential-diffusion conditions. Another feature of the results illustrated in Fig. 6 is that stretch causes the maximum laminar burning velocity condition to shift toward the negative Markstein number region. The predictions using the Mueller et al. [23] reaction mechanism represent these combined reaction and transport effects quite well.

Flame-Structure/Stretch Interactions

As discussed earlier, measurements and predictions of $S_{L\infty}$ and Ma are in reasonably good agreement over the present test range; therefore, the predictions were exploited to seek improved understanding about flame/stretch interactions. Results of this type for argon-diluted flames at NTP are discussed in the following based on the Mueller et al. [23] reaction mechanism. Corresponding results based on the mechanisms of Marinov et al. [24] and Fren-

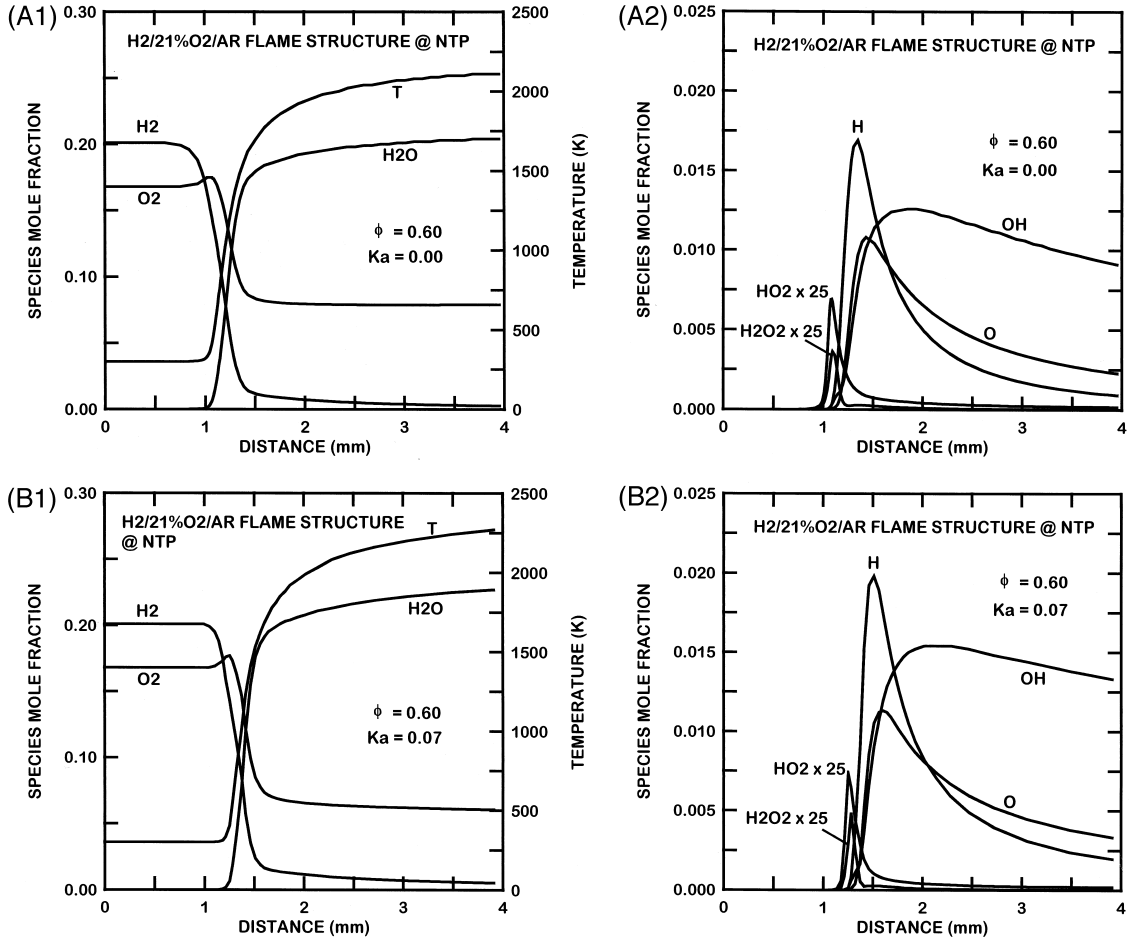

Fig. 7. a Predicted structure of an unstretched (Ka = 0) H_2/21% O_2/Ar flame at NTP for an unstable preferential-diffusion condition ($\phi = 0.6$). Based on the kinetics of Mueller et al. [23]. Fig. 7b Predicted structure of a stretched (Ka $\approx$ 0.07) H_2/21% O_2/Ar flame at NTP for an unstable preferential-diffusion condition ($\phi = 0.6$). Based on the kinetics of Mueller et al. [23].

klach et al. [25, 26] were similar. These results were also similar to hydrogen/air flames because these flames have similar transport properties, as discussed earlier. The approach involved numerical simulations of outwardly propagating spherical flames for unstable ($\phi = 0.6$) and stable ($\phi = 4.5$) preferential-diffusion conditions. Flame-structure/stretch interactions were observed by comparing results for a moderate level of stretch (Ka = 0.07) with corresponding predictions for unstretched (plane) flames (Ka = 0).

Typical predicted structures of stretched and unstretched laminar premixed H_2/21% O_2/Ar flames at NTP are illustrated in Figs. 7 and 8 for fuel-lean (unstable) and fuel-rich (stable) conditions, respectively. Results illustrated in the figures include distributions of temperature and species mole fractions as a function of distance although the flame. It should be noted that the origins of the length scales for both unstretched and stretched flames in these figures are arbitrary and the latter do not correspond to the central ignition point. The results show that maximum concentrations of the radicals HO_2 and H_2O_2 are roughly two orders of magnitude smaller than those of H, OH, and O; therefore, the latter tend to dominate reactive effects in the present flames.

Considering the results for the fuel-lean (unstable) flame in Fig. 7, finite levels of stretch cause flame temperatures to increase. This occurs because the faster-diffusing hydrogen compared to oxygen causes the flame to become

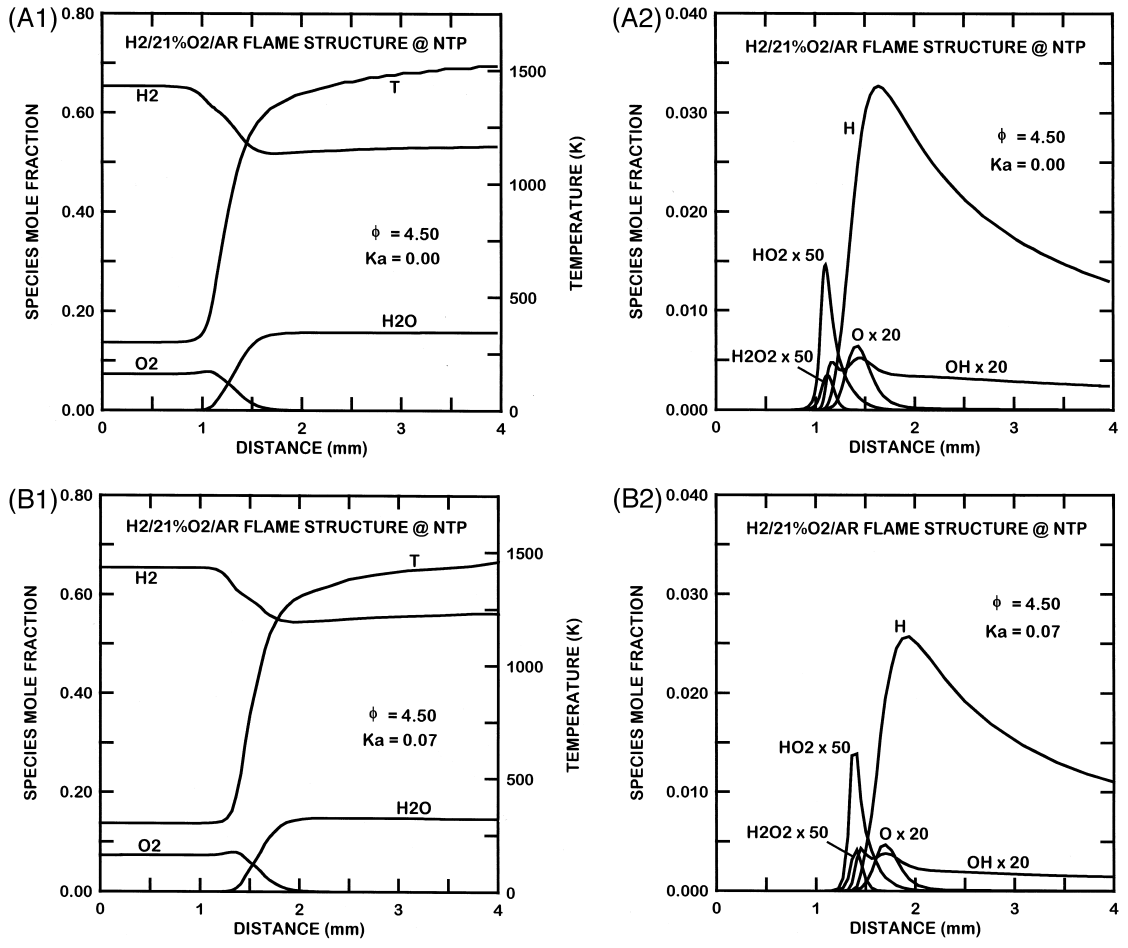

Fig. 8. a Predicted structure of an unstretched (Ka = 0) H_2/21% O_2/Ar flame at NTP for a stable preferential-diffusion condition ($\phi = 4.5$). Based on the kinetics of Mueller et al. [23]. Fig. 8b Predicted structure of a stretched (Ka $\approx$ 0.07) H_2/21% O_2/Ar flame at NTP for a stable preferential-diffusion condition ($\phi = 4.5$). Based on the kinetics of Mueller et al. [23].

more nearly stoichiometric (note the reduced concentrations of oxygen and increased concentrations of water vapor at the hot boundary of the stretched flame compared to the unstretched flame); this causes a corresponding increase of the flame temperature of the stretched flame compared to the unstretched flame. The increased temperature (and possibly increased concentrations of light radicals such as hydrogen atom and hydroxyl radical) causes radical concentrations, particularly the major radicals H, OH, and O, in the reaction zone of the stretched flame to increase compared to the unstretched flame (e.g., the maximum mole fraction of H in the stretched and unstretched flames are roughly 0.020 and 0.017, respectively), increasing reaction rates and thus laminar burning velocities for the stretched flame.

The effect of stretch on flame structure for fuel-rich (stable) conditions is just opposite to the behavior just discussed for unstable conditions (compare Figs. 7 and 8). For stable conditions, finite levels of stretch cause flame temperatures to decrease. This occurs because the faster-diffusing hydrogen compared to oxygen causes the flame to become even richer (note the increased concentrations of H_2 and decreased concentrations of water vapor at the hot boundary of the stretched flame compared to the unstretched flame); this causes a corresponding reduction of the flame temperature of the stretched flame compared to the un-

stretched flame. The reduced temperature (somewhat opposed by increased H and OH concentrations) causes radical concentrations in the reaction zone of the stretched flame to decrease compared to the unstretched flame (e.g., the maximum mole fractions of H in the stretched and unstretched flames are roughly 0.026 and 0.033, respectively), decreasing reaction rates and thus laminar burning velocities for the stretched flames.

Effects of flame structure on H_2/21% O_2/Ar flames at NTP are more complex at intermediate fuel-equivalence ratios near the maximum laminar burning velocity condition. This occurs because the variation of laminar burning velocity with fuel-equivalence ratio is small in this region which suggests that preferential diffusion of a light fuel species such as H_2 is not an important factor in flame/stretch interactions. For example, predicted structures of stretched and unstretched laminar premixed H_2/21% O_2/Ar flames at $\phi = 1.8$ and NTP, as a typical intermediate condition, exhibited only small changes (reductions) of temperature and radical concentrations for stretched flames compared to the corresponding unstretched flames, i.e., profiles of temperature and radical concentrations of stretched and unstretched flames were nearly identical despite having a relatively large value of the Markstein number (Ma = 3.4) at this condition. This occurs because effects of fuel-equivalence ratio on the laminar burning velocity at this maximum laminar burning velocity condition are weaker than for more fuel-lean and fuel-rich conditions, so that effects of preferential diffusion of mass and heat, as well as the tendency for light radical concentrations to increase in the reaction zone of stretched flames (which opposes effects of preferential diffusion of mass and heat at the present intermediate condition) become factors in addition to effects of preferential diffusion of mass that were just discussed for more fuel-lean and fuel-rich conditions.

Based on these observations, it is interesting to study the relative sensitivities of the present flames to effects of preferential diffusion of mass and heat. This is illustrated by the plots in Fig. 9 of the ratio of normalized mass and thermal sensitivities of laminar burning velocities for H_2-fueled flames at NTP having various

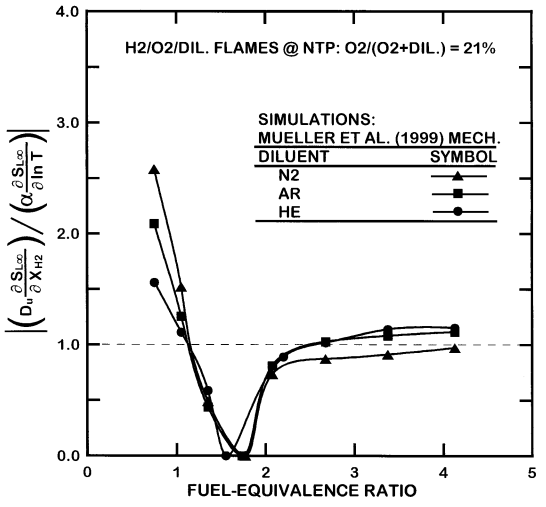

Fig. 9. Ratio of normalized mass and thermal sensitivities of laminar burning velocity for hydrogen-fueled flames at NTP. Based on the kinetics of Mueller et al. [23].

diluents over the present range of fuel-equivalence ratios. The ratio of the mass/thermal sensitivities behaves in a similar manner for the three diluents, particularly for fuel-rich conditions; this behavior is similar to the behavior of Ma for these conditions seen in Fig. 4. The general behavior is that the ratio is greater than unity for fuel-lean conditions, which suggests that preferential diffusion of mass is somewhat more important than the preferential diffusion of heat in this region. It is not surprising, however, that thermal sensitivity at lean conditions is somewhat increased for the helium-diluted flames due to the relatively large transport rates of helium. Then, near the maximum laminar burning velocity condition (ϕ of 1.6–1.8), the sensitivity of the flames to variations of fuel-equivalence ratios becomes small, so that stability is dominated by preferential diffusion of heat. Finally, at fuel-rich conditions preferential diffusion of mass and heat make comparable contributions to preferential-diffusion/stretch interactions of these flames. This behavior highlights the complexity of flame/stretch interactions when preferential diffusion of various species and heat tends to dominate different ranges of fuel-equivalence ratios for given reactant temperatures, pressures, and diluent concentrations.

The maximum laminar burning velocities of

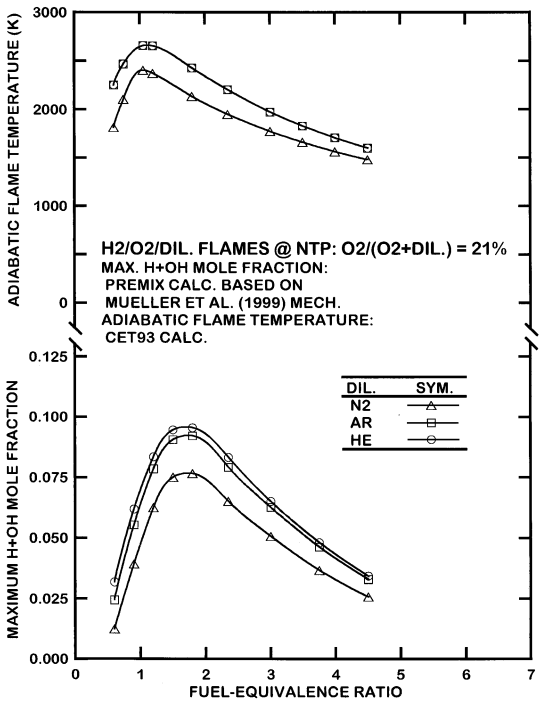

Fig. 10. Predicted maximum H+OH mole fraction in the reaction zone and adiabatic flame temperature as a function of fuel-equivalence ratio for hydrogen-fueled flames at NTP. Based on the kinetics of Mueller et al. [23].

H_2/21% O_2/diluent (N_2, Ar or He) flames at NTP occur at $\phi \approx 1.6$ to 1.8 which is far from the maximum flame temperature condition of $\phi \approx 1.0$ (stoichiometric condition). This can be explained by consideration of light radical (H and OH) concentrations based on the computed flame structure. The mole fraction of H+OH at the position of the maximum mole fraction of H in the flame was obtained from the computed structure of unstretched H_2/21% O_2/diluent (N_2, Ar or He) flames at NTP (e.g., see the unstretched flame structures in Figs. 7 and 8) and the corresponding adiabatic flame temperatures were calculated using the algorithms of McBride et al. [27] and Reynolds [28]. These results are plotted in Fig. 10. Although the flame temperature reaches a maximum value near $\phi = 1.0$, the H+OH radical concentration reaches a maximum value for $\phi \approx 1.6$ to 1.8. Thus, the maximum laminar burning velocities of H_2/21% O_2/diluent (N_2, Ar or He) flames at NTP at $\phi \approx 1.6$ to 1.8 are associated with maximum concentrations of H+OH radicals at the same condition, with the radicals promoting higher reaction rates as discussed by Padley and Sudgen [38]. In addition, the present results support the correspondence between the maximum laminar burning velocity and the maximum hydrogen radical concentration, at a particular fuel-equivalence ratio, originally postulated by Warnatz [39]; the reason why the hydroxyl radical as well as the hydrogen radical were considered during the present investigation will be explained later when more detailed discussion about effects of radicals on laminar burning velocities is undertaken.

Results at Normal Temperature and Various Pressures and Dilutions

Most practical premixed flames operate at considerably larger flame temperatures and pressures than the test conditions considered in the previous section; therefore, it is interesting to study whether the substantial preferential-diffusion/stretch interactions of the present hydrogen-fueled flames with reactants at NTP conditions persist to practical flame conditions. Effects of pressure and temperature on flame sensitivity to preferential-diffusion/stretch interactions for $H_2/O_2/N_2$ flames were investigated by Aung et al. [19]. They presented extensive results for $H_2/O_2/N_2$ flames having various fuel-equivalence ratios at pressures of 0.35 to 4.00 atm and various oxygen concentrations, e.g., $O_2/(O_2+N_2) = 0.125$ to 0.210 by volume. Thus, to extend the results due to Aung et al. [19] and to gain more insight about this issue, effects of flame temperature and pressure on the sensitivity of hydrogen-fueled flames to preferential-diffusion/stretch interactions were studied both experimentally and computationally considering H_2/O_2/diluent (Ar or He) reactant mixtures at $\phi = 0.6$ and 4.5. This information was obtained by changing flame temperatures by changing O_2 concentrations in the nonfuel gases for H_2/O_2/Ar mixtures at NTP, and by changing flame pressures for H_2/21% O_2/diluent (Ar or He) mixtures at normal temperature (NT). These results will be considered next.

Effects of Pressure on Flame Response to Stretch

Effects of pressure on flame response to stretch are summarized in Tables 2 and 3 for H_2/21%

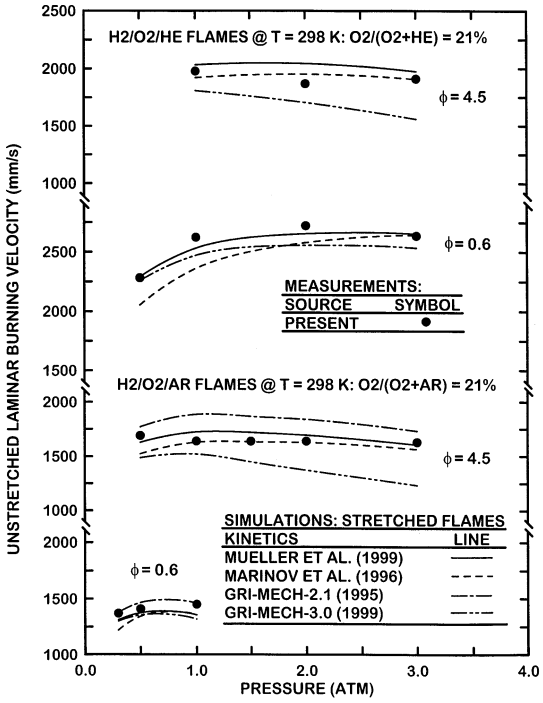

Fig. 11. Effect of pressure on measured and predicted unstretched laminar burning velocities of H_2/21% O_2/diluent (Ar or He) flames at fuel-equivalence ratios of 0.6 and 4.5, and a temperature of 298 K. Predictions based on the kinetics of Mueller et al. [23].

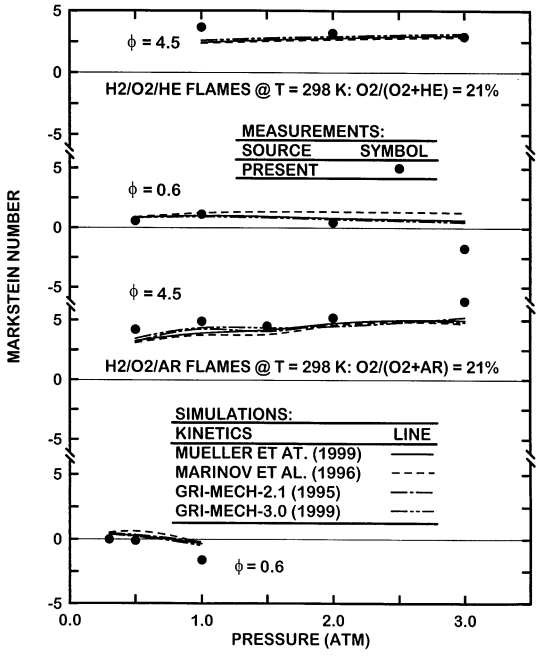

Fig. 12. Effect of pressure on measured and predicted Markstein numbers of H_2/21% O_2/diluent (Ar or He) flames at fuel-equivalence ratios of 0.6 and 4.5, and a temperature of 298 K. Predictions based on the kinetics of Mueller et al. [23].

O_2/Ar and H_2/21% O_2/He flames, respectively, and are illustrated by plots of unstretched laminar burning velocities and Markstein numbers as a function of pressure in Figs. 11 and 12. The procedures to obtain these two parameters and the general results are the same as those for NTP conditions, i.e., there was a linear relationship between $S_{L\infty}/S_L$ and Ka so that Ma was independent of Ka over the range of present measurements for a given mixture composition and pressure. In contrast to the observations for hydrocarbon/air flames [20–22], which showed a progressive reduction of $S_{L\infty}$ with the increasing flame pressure due to increased rates of three-body recombination reactions, the pressure dependence of $S_{L\infty}$ for H_2/21% O_2/diluent (Ar or He) flames is small based on the results illustrated in Fig. 11, similar to past observations for the hydrogen/air flames [19]. Based on numerical simulations at various fuel-equivalence ratios and pressures for laminar premixed hydrogen/air flames, Sun et al. [13] showed that the pressure dependence of $S_{L\infty}$ for these hydrogen-fueled flames is somewhat complicated, e.g., the pressure exponent depends on the mixture compositions as well as the pressure range; therefore, it is difficult to find a general relationship between laminar burning velocities and pressure. The measurements generally agree with all the simulated results within experimental uncertainties for the present pressure range, except for the predictions based on Frenklach et al. [26] mechanism for fuel-rich conditions at high pressures. The mechanism of Mueller et al. [23], however, is seen to provide the best quantitative predictions of $S_{L\infty}$ over the entire test range of Fig. 11, similar to the observations at NTP conditions.

The associated variation of Markstein numbers with increasing pressure in Fig. 12 is very similar to past observations for the hydrogen/air flames by Aung et al. [19]: measurements and predictions agree reasonably well and pressure variations do not have a large effect on Markstein number values for pressures in the range 0.3 to 3.0 atm. The latter observation is somewhat different from that for hydrocarbon/air

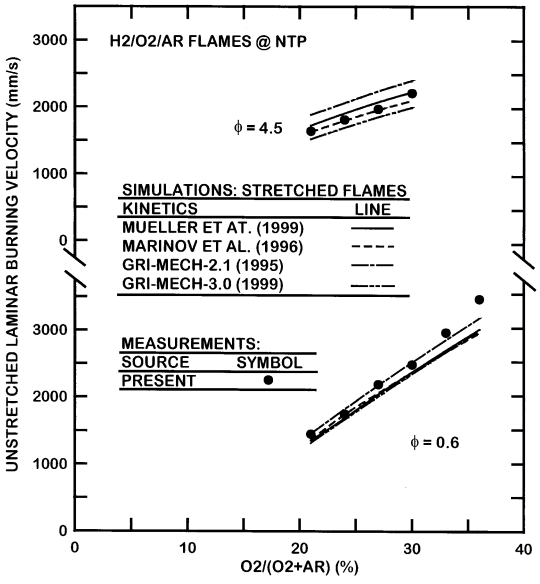

Fig. 13. Effect of oxygen concentration on measured and predicted laminar burning velocities of $H_2/O_2/Ar$ flames at fuel-equivalence ratios of 0.6 and 4.5, and NTP. Predictions based on the kinetics of Mueller et al. [23].

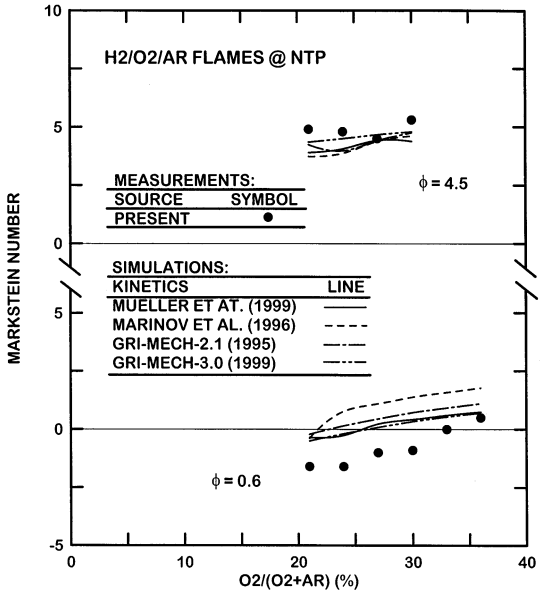

Fig. 14. Effect of oxygen concentration on measured and predicted Markstein numbers of $H_2/O_2/Ar$ flames at fuel-equivalence ratios of 0.6 and 4.5, and NTP. Predictions based on the kinetics of Mueller et al. [23].

flames [20–22] that exhibit a progressive reduction of Markstein numbers with increasing pressure. Another finding from Fig. 12 is that the flames tend to become preferential-diffusion unstable with increasing pressure at fuel-lean conditions. Comparing the images of the unstable flames at an atmospheric pressure and at pressure of 2 atm for H_2/21% O_2/Ar flames at a fuel-lean condition ($\phi = 0.6$) suggested that an increase of pressure could make the flame significantly more unstable at fuel-lean conditions, despite a small change of Ma. On the other hand, a similar comparison for a fuel-rich condition ($\phi = 4.5$) showed no significant change of either flame behavior or Ma values.

Effects of Temperature on Flame Response to Stretch

Effects of flame temperature (by varying O_2 concentrations in the nonfuel gases at NTP) on flame response to stretch are summarized in Table 2 for $H_2/O_2/Ar$ flames at NTP, with unstretched laminar burning velocities and Markstein numbers illustrated as a function of oxygen concentration in the nonfuel gases in Figs. 13 and 14. As discussed in the previous section, the procedures to obtain these two parameters and the general results are the same as those at NT and various pressures, i.e., there was a linear relationship between $S_{L\infty}/S_L$ and Ka which implies Ma independent of Ka over the range of present measurements for given reactant conditions. Similar to the observations for alkane-vapor/air flames [22], increasing the flame temperature by increasing the oxygen concentration yields a corresponding increase of $S_{L\infty}$ (Fig. 13). This behavior follows because increased flame temperatures at a fixed pressure tend to increase radical concentrations in the reaction zone of the flame. Then, based on the proportionality between radical concentrations in the reaction zone and laminar burning velocities, mentioned earlier, laminar-burning velocities increase accordingly. The measurements generally agree with all the simulated results within experimental uncertainties for the present oxygen concentration range, except for the predictions at fuel-lean conditions and high oxygen concentrations. Different from results for previous predictions during the present investigation, the mechanism of Mueller et al. [23] does not provide the best quantitative predictions in Fig. 13; the Frenklach et al. [25], and Marinov et al. [24] mechanisms appear to be

better for fuel-lean and fuel-rich conditions, respectively; nevertheless, the discrepancies between measurements and predictions in Fig. 13 are not very large.

The corresponding variation of Markstein numbers with increasing flame temperatures seen in Fig. 14 exhibits trends similar to pressure changes: a small trend of increasing Ma with increasing oxygen concentration for fuel-lean conditions whereas no significant change for fuel-rich conditions. Comparing the behavior of H_2/O_2/Ar flames at this fuel-lean condition with that for alkane-vapor/O_2/N_2 flames at NTP [22] indicates that increasing the oxygen concentration in a mixture makes the flame less sensitive to stretch at these conditions. Finally, the agreement between measurements and predictions of Ma for fuel-lean conditions with changing oxygen concentrations is worse than any other previous cases considered during the present investigation, even although these predictions still follow the general trend of the measurements. This discrepancy could be mainly caused by increased uncertainties of data reduction for these unstable and near-neutral preferential-diffusion conditions, as noted earlier.

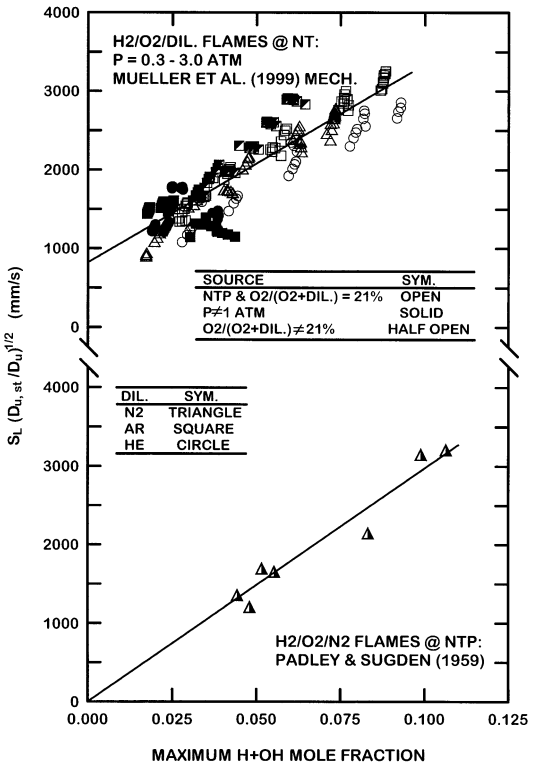

Fig. 15. Computed laminar burning velocities as a function of computed maximum H+OH mole fraction in the reaction zone for hydrogen-fueled flames at a temperature of 298 K. Based on the kinetics of Mueller et al. [23].

H and OH Radical Behavior

The flame structure results illustrated in Figs. 7 and 8 indicate that H-atom has the largest concentrations of all radicals in the reaction zone of the present flames, even for lean flames with fuel-equivalence ratios as small as $\phi = 0.6$ which is the smallest value considered during the present study. In addition, OH radical concentrations are comparable to H-atom concentrations for fuel-lean flames. This behavior is significant because Padley and Sugden [38] have established a strong correlation between laminar burning velocities and H-atom concentrations for $H_2/O_2/N_2$ flames based on their direct measurements of radial concentrations and the laminar burning velocity measurements of Jahn [40]. In addition, Butler and Hayhurst [41] developed a simplified theory that yields a strong correlation between laminar burning velocities and H-atom concentrations for fuel-rich $H_2/O_2/N_2$ flames, similar to Padley and Sugden [38]. These results show that other factors, such as diffusivity of H-atom, O_2 concentrations in the unburned gas mixture and the reaction rate constant of $H+O_2 \rightarrow OH+O$, are involved in the correlation of laminar burning velocities, along with H-atom concentrations. Combining these observations with the fact that H-atom has significantly larger diffusivities than other species and heat in the present H_2/O_2/diluent (N_2, Ar or He) flames tends to implicate H and/or OH radicals as important factors in the relatively strong flame/stretch interactions observed for present test conditions. The following discussion seeks to quantify this H and/or OH radical preferential-diffusion mechanism.

Present computations were used to study the correlation between laminar burning velocities and mole fractions of H+OH at the position of maximum mole fraction of H-atom in the flame. These results are illustrated in Fig. 15. The laminar burning velocities illustrated in this figure have been normalized by multiplying

$(D_{u,st}/D_u)^{1/2}$, where $D_{u,st}$ and D_u are a standard mass diffusivity between hydrogen and nitrogen and a mass diffusivity between hydrogen and diluent considered at a given temperature and pressure, respectively. The resulting normalized laminar burning velocities were used to obtain a single correlation for all the diluted flames, based on simple phenomenological analysis of premixed flames which suggests that $S_L \sim D_u^{1/2}$, see Turns [42]. Present predictions shown on the plot involve all fuel-equivalence ratios, pressures and oxygen concentrations for flames using nitrogen, argon and helium as diluents, and include results for both unstretched and stretched flames. This large range of conditions yields a somewhat scattered but still quite strong correlation between normalized laminar burning velocities and maximum H+OH mole fractions. The correlation with the H-atom concentration alone was also considered but the resulting correlation was more scattered than the correlation illustrated in Fig. 15. This selection of maximum H+OH radical concentration can also be justified based on earlier observations of these radical distributions in the flames for fuel-lean conditions. Finally, the present correlation is qualitatively similar to the correlation initially proposed by Padley and Sugden [38] based on measured laminar burning velocities and radical concentrations; this correlation is also shown on the plot.

The behavior observed in Fig. 15 suggests that maximum H+OH radical concentrations could serve as a surrogate for the laminar burning velocity when considering flame/stretch interactions. This behavior is explored in Fig. 16 where the ratios of the unstretched-to-stretched maximum H+OH mole fractions are plotted as a function of Karlovitz numbers, analogous to the plot of $S_{L\infty}/S_L$ as a function of Karlovitz number in Figs. 1 through 3. Effects of diluent are also shown on the plot, based on results for hydrogen/air, H_2/21% O_2/Ar and H_2/21% O_2/He flames at NTP. Three sets of results are shown for flames involving each diluent, for fuel-equivalence ratios of 0.6, 1.8, and 4.5; results for other conditions are similar. Remarkably, these plots are linear, similar to the laminar burning velocity results of Figs. 1 through 3. This behavior suggests defining an expression

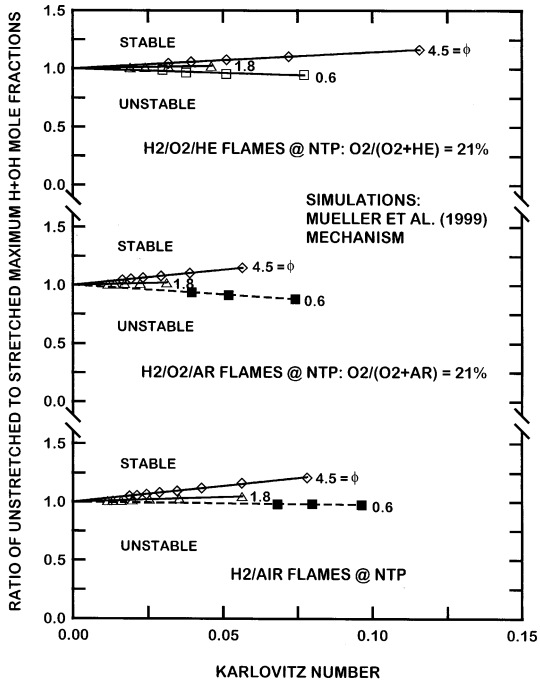

Fig. 16. Predicted maximum H+OH mole fraction in the reaction zone as a function of Karlovitz number and fuel-equivalence ratio for hydrogen-fueled flames at NTP. Based on the kinetics of Mueller et al. [23].

for the effects of stretch on maximum H+OH mole fractions, analogous to Eq. 1, as follows:

$$X_{(H+OH)max\,\infty}/X_{(H+OH)max} = 1 + Ma_{H+OH}Ka \quad (4)$$

The behavior of Ma_{H+OH} was studied by plotting the correlation between Ma_{H+OH} and Ma as illustrated in Fig. 17. Results shown on the plot consider the full range of present test conditions at normal temperature. Based on the results illustrated in Fig. 16, the correlation of Fig. 17 includes stretched flames, extending up to the maximum stretch values considered during the present investigation. The strong correlation between Ma and Ma_{H+OH} is evident, if one data point having the largest negative value of Ma is excluded (this data point has the largest uncertainty among all the data shown in the plot due to the nature of Ma, as noted earlier), supporting the importance of H and OH radical concentrations for preferential diffusion effects that cause the flame/stretch interactions observed during the present investigation. These results suggest, however, that other factors are

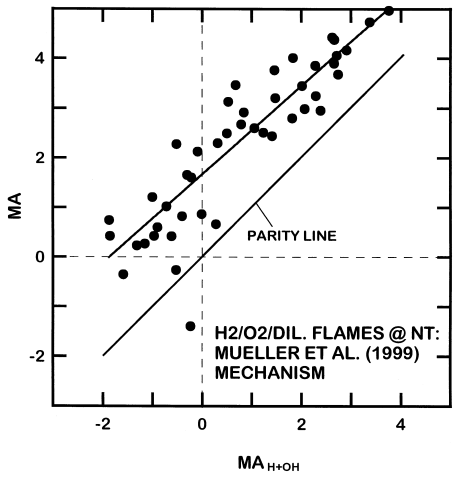

Fig. 17. Correlation between Ma and Ma_{H+OH} for hydrogen-fueled flames at a temperature of 298 K. Based on the kinetics of Mueller et al. [23].

involved, e.g., conditions where Ma and $Ma_{H+OH} = 0$ do not coincide (compare the correlation line and the parity line in Fig. 17). Of course, this discrepancy between the two lines is an expected result because the present correlation line between normalized laminar burning velocities and maximum H+OH mole fractions, illustrated in Fig. 15, does not pass through the origin in contrast to the correlation line reported by Padley and Sugden [38]. Thus, additional study is needed to better understand the mechanism of flame/stretch interactions, and the role of radical concentrations in these interactions, even for relatively simple H_2/O_2/diluent flames.

CONCLUSIONS

Effects of positive flame stretch on the laminar burning velocities of H_2/O_2/diluent (N_2, Ar or He) flames were studied experimentally and computationally. The experiments involved outwardly propagating spherical laminar premixed flames, while the computations involved numerical simulations of the same flame configuration considering the detailed chemical reaction mechanisms of Mueller et al. [23], Marinov et al. [24], and Frenklach et al. [25, 26]. The test conditions included fuel-equivalence ratios of 0.6 to 4.5, pressures of 0.3 to 3.0 atm, volumetric oxygen concentrations in the nonfuel gases of 0.21 to 0.36, and Karlovitz numbers of 0 to 0.5, at normal temperatures. The major conclusions of the study are as follows:

1. Effects of flame/stretch interactions for both measurements and predictions could be correlated based on the local conditions hypothesis according to $S_{L\infty}/S_L = 1 + MaKa$ to obtain a linear relationship between $S_{L\infty}/S_L$ and Ka, yielding constant Markstein numbers for given reactant conditions.
2. Effects of flame stretch on laminar burning velocities were substantial, yielding values of $S_{L\infty}/S_L$ in the range 0.6 to 3.0, even though present flames did not approach quenching conditions; corresponding Markstein numbers were in the range–3 to 7.
3. Predicted and measured unstretched laminar burning velocities and Markstein numbers were generally in good agreement using the contemporary H_2/O_2 chemical reaction mechanisms [23–26]; nevertheless, discrepancies among the various predictions and measurements at some test conditions, e.g., fuel-lean conditions with large oxygen concentrations, merit additional consideration.
4. Various diluents (N_2, Ar, and He) highlight effects of transport and chemistry on preferential-diffusion/stretch interactions. Replacing nitrogen with argon yielded larger laminar burning velocities due to increased flame temperatures but had a relatively small effect on Markstein numbers due to nearly same transport properties for the two diluents. Replacing nitrogen with helium, however, yielded a larger laminar burning velocities due to both increased flame temperatures and transport rates, and also stabilized lean flames by enhancing the diffusion of heat.
5. Effects of pressure and argon-dilution on both the magnitude and trends of Markstein numbers were small for fuel-rich conditions. These effects were modest for fuel-lean conditions but there was reduced flame sensitivity to stretch with increasing flame temperatures and increased tendencies toward preferential-diffusion instability behavior with increasing pressures, similar to the past observations of alkane-vapor-fueled flames [22].
6. Predictions show that stretched flames ex-

hibit a strong correlation between laminar burning velocities and maximum H+OH radical concentrations, similar to the measurements of Padley and Sugden [38] in similar flames.

7. The local conditions hypothesis provides a simple correlation between the ratio of unstretched to stretched maximum H+OH mole fractions and the Karlovitz number similar to the behavior of laminar burning velocities, yielding constant H+OH Markstein numbers (Ma_{H+OH}) for particular reactant conditions. The corresponding strong correlation between Ma and Ma_{H+OH} suggests that H and OH radical production and transport are important aspects of preferential-diffusion/stretch interactions. This behavior is not surprising, however, in view of the unusually large diffusivities and strong effects on laminar burning velocities of these light radicals.

This research was supported in part by NSF Grant CTS-9321959 under the Technical Management of F. Fisher. Support from the Rackham Fellowship Program of the University of Michigan for O. C. Kwon is also gratefully acknowledged. Thanks are also due to Dr. N. M. Marinov of Sandia National Laboratories for providing an updated version of the hydrogen/oxygen reaction mechanism of Marinov et al. [24].

REFERENCES

1. Manton, J., von Elbe, G., and Lewis, B. *J. Chem. Phys.* 20:153 (1952).
2. Markstein, G. H., *Non-Steady Flame Propagation*, Pergamon, New York, p. 22, 1964
3. Strehlow, R. A., and Savage, L. D. *Combust. Flame* 31:209 (1978).
4. Clavin, P. *Prog. Energy Combust. Sci.*11:1 (1985).
5. Law, C. K. *Proc. Combust. Inst.* 22:1381 (1988).
6. Taylor, S. C., Ph. D. thesis, University of Leeds, England, U. K., 1991.
7. Dowdy, D. R., Smith, D. B., Taylor, S. C., and Williams, A. *Proc. Combust. Inst.* 23:325 (1990).
8. Brown, M. J., McLean, I. C., Smith, D. B., and Taylor, S. C. *Proc. Combust. Inst.* 26:875 (1996).
9. Karpov, V. P., Lipatnikov, A. N., and Wolanski, P. *Combust. Flame* 109:436 (1996).
10. Bradley, D., Hicks, R. A., Lawes, M., Sheppard, C. G. W., and Woolley, R. *Combust. Flame* 115:126 (1998).
11. Egolfopoulos, F. N., and Law, C. K. *Proc. Combust. Inst.* 23:333 (1990).
12. Vagelopoulos, C. M., Egolfopoulos, F. N., and Law, C. K. *Proc. Combust. Inst.* 25:1341 (1994).
13. Sun, C. J., Sung, C. J., He, L., and Law, C. K. *Combust. Flame* 118:108 (1999).
14. Aung, K. T., Hassan, M. I., Kwon, S., Tseng, L. -K., Kwon, O. C., and Faeth, G. M. *Combust. Sci. Tech.*, in press.
15. Kwon, S., Tseng, L.-K., and Faeth, G. M. *Combust. Flame* 90:230 (1992).
16. Tseng, L.-K., Ismail, M. A., and Faeth, G. M. *Combust. Flame* 95:410 (1993).
17. Aung, K. T., Hassan, M. I., and Faeth, G. M. *Combust. Flame* 109:1 (1997).
18. Hassan, M. I., Aung, K. T., and Faeth, G. M., J. *Prop. Power* 13:239,(1997).
19. Aung, K. T., Hassan, M. I., and Faeth, G. M. *Combust. Flame* 112:1, (1998).
20. Hassan, M. I., Aung, K. T., and Faeth, G. M. *Combust. Flame* 115:539 (1998).
21. Hassan, M. I., Aung, K. T., Kwon, O. C, and Faeth, G. M. *J. Prop. Power* 14:479 (1998).
22. Kwon, O. C., Hassan, M. I., and Faeth, G. M. *J. Prop. Power* 16:513 (2000).
23. Mueller, M. A., Kim, T. J., Yetter, R. A., and Dryer, F. L. *Int. J. Chem. Kinetics* 31:113 (1999).
24. Marinov, N. M., Westbrook, C. K., and Pitz, W. J. in *Transport Phenomena in Combustion*, Vol. I (S. H. Chan, Ed.), Taylor & Francis, Washington, D. C., 1996, p. 118.
25. Frenklach, M., Wang, H., Bowman, C. T., Hanson, R. K., Smith, G. P., Goldin, D. M., Gardiner, W. C., and Lissianski, V. World Wide Web location http. //www.me.berkeley.edu/gri mech/, Version 2.1, 1995.
26. Frenklach, M., Bowman, C. T., Smith, G. P., and Gardiner, W. C. World Wide Web location http. //www.me.berkeley.edu/gri mech/, Version 3.0, 1999.
27. McBride, B. J., Reno, M. A., and Gordon, S. *CET93 and CETPC. An Interim Updated Version of the NASA Lewis Computer Program for Calculating Complex Chem Equilibrium with Applications*, NASA Report No. TM-4557, 1994.
28. Reynolds, W. C. *The Element Potential Method for Chemical Equilibrium Analysis. Implementation in the Interactive Program STANJAN*, Department of Mechanical Engineering Report, Stanford University, Stanford, CA, 1986.
29. Kim, T. J., Yetter, R. A., and Dryer, F. L. *Proc. Combust. Inst.* 25:759 (1994).
30. Wang, W., and Rogg, B. *Combust. Flame* 94:271 (1993).
31. Kwon, O. C., Ph. D. thesis, University of Michigan, Ann Arbor, Michigan, 2000.
32. Rogg, B. *RUN-1DL. The Cambridge Universal Laminar Flame Code*, Technical Report CUED/A-THERMO/TR39, Department of Engineering, University of Cambridge, England, U. K., 1991.
33. Kee, R. J., Rupley, F. M., and Miller, J. A. *The CHEMKIN Thermodynamic Data Base*, Sandia National Laboratories Report No. SAND87–8215B, 1992.
34. Kee, R. J., Rupley, F. M., and Miller, J. A. *CHEMKIN*

II. A Fortran Chemical Kinetics Package for the Analysis of Gas Phase Chemical Kinetics, Sandia National Laboratories Report No. SAND89–8009B, 1993.
35. Kee, R. J., Dixon-Lewis, G., Warnatz, J., Coltrin, M. E., and Miller, J. A. *A FORTRAN Computer Code Package for the Evaluation of Gas-Phase, Multi-component Transport Properties*, Sandia National Laboratories Report No. SAND86–8246, 1992.
36. Kee, R. J., Grcar, J. F., Smooke, M. D., and Miller, J. A. *A FORTRAN Program for Modeling Steady Laminar One-Dimensional Premixed Flames*, Sandia National Laboratories Report No. SAND85–8240, 1993.
37. Groff, E. G. *Combust. Flame* 48:51 (1982).
38. Padley, P. J., and Sugden, T. M. *Proc. Combust. Inst.* 7:235 (1959).
39. Warnatz, J. *Combust. Sci. Tech.* 26:203 (1981).
40. Jahn, G., cited in Lewis, B, and von Elbe, G. *Combustion, Flames and Explosions of Gases,* 3rd ed., Academic Press, New York, p. 395, 1987.
41. Butler, C. J., and Hayhurst, A. N. *Combust. Flame* 115:241 (1998).
42. Turns, S. R. *An Introduction to Combustion: Concepts and Applications, 2nd ed.*, McGraw–Hill, New York, 2000, p. 261.

Received 6 May 2000 ; revised 22 September 2000; accepted 4 October 2000